Contract No.:

This manuscript has been authored by Savannah River Nuclear Solutions (SRNS), LLC under Contract No. DE-AC09-08SR22470 with the U.S. Department of Energy (DOE) Office of Environmental Management (EM).

Disclaimer:

Insights into the Thermal Decomposition of Plutonium(IV) Oxalate – A DFT Study of the Intermediate Structures

*Christopher J. South and Lindsay E. Roy**

Contributions from Savannah River National Laboratory, P. O. Box A, Aiken, SC 29808

RECEIVED DATE (to be automatically inserted after your manuscript is accepted if required according to the journal that you are submitting your paper to)

Keywords: plutonium, actinide, decomposition, DFT, solid state, computational, crystal structure, oxidation state

* To whom correspondence should be addressed (lindsay.roy@srnl.doe.gov)

Abstract

The thermal decomposition of plutonium oxalate to oxide is one of the most studied reactions in actinide chemistry but the intermediates have been the subject of debate for decades. Recent experimental data suggest that the decomposition of Pu(IV) oxalate in air undergoes dehydration first, then reduction to Pu(III) oxalate. The precise structural modifications that take place are unknown as experiments have not been able to fully characterize the intermediates at the microscopic level. To rectify this, we employed solid state density functional theory calculations at the PBE-D3 level with a Hubbard U correction to model the structures and energetics of potential dehydrated Pu(IV) and Pu(III) oxalate intermediate compounds. Based on the theoretical study presented here, the anhydrous analogues of the known hydrated Pu(IV) and Pu(III) oxalates are the preferred crystal structures formed through an overall exothermic reaction process. However, decomposition could proceed through the formation of a higher energy, more complicated 3D lattice structure with frustrated oxalate binding. It is expected that the intermediates presented here could be identified using spectroscopic techniques to enable further insight into the reaction mechanism.

1: Introduction

The complex mechanism associated with the conversion of actinide oxalates to oxides presents an interesting scientific and technological problem given its importance in nuclear separations. Similar to transition metal chemistry, the simple decomposition reaction is complicated by not only rich redox chemistry afforded by the metal center, but also the atmospheric conditions during the reaction. The most studied reaction in the actinide series involves plutonium which is particularly interesting since it straddles the series with respect to bonding and oxidation state. The chemical route starts from plutonium oxalate in either the +3 or +4 oxidation state leading to the formation of Pu(IV) dioxide and other gaseous products (H_2O, CO_2, CO). However, identification of the intermediates has been an area of debate in the literature, especially when starting from Pu(IV) oxalate.[1] Myers was the first to note reduction to a Pu(III) oxalate intermediate after initial dehydration.[2] Rao, Subramanian, and Welch partially agreed with an observed Pu(III) intermediate but identified the species as $Pu_2(C_2O_4)_2(CO_3)$.[3] Later work by Jenkins and Waterman presented contradictory evidence that decomposition does not undergo a reduction step and instead proposed a $Pu(IV)(CO_3)_2$ species.[4] Glasner then added that these observed differences in the stabilities of the Pu(III) intermediate are a result of the decomposition reaction occuring in the presence or absence of air.[5] Nissen also proposed that $Pu_2(C_2O_4)_3$ is an intermediate product in the decomposition reaction occurring under argon.[6]

Most recently, Vigier *et al.* analyzed the conversion of Pu(IV) oxalate to oxide under both air and argon using thermogravimetric analysis.[7] Interestingly, the diagrams show that there are different reaction pathways for the two different atmospheres. Infrared and UV-vis spectroscopies were used to identify several intermediates, including $Pu_2(C_2O_4)_3$ as a transitory species under both air and argon. The proposed mechanism can be found in Scheme 1, with Vigier noting that the anhydrous species could not be rigorously isolated and characterized due to the hygroscopic nature of the material.[7] As shown, the presence of a Pu(III) oxalate intermediate implies that metal reduction plays a vital role in the calcination reaction pathways.[8] With additional work by de Almeida *et al.* on the calcination of Pu(III) oxalate, the reaction pathway is assumed to proceed through complete dehydration of the oxalate intermediate prior to ligand decomposition.[8]

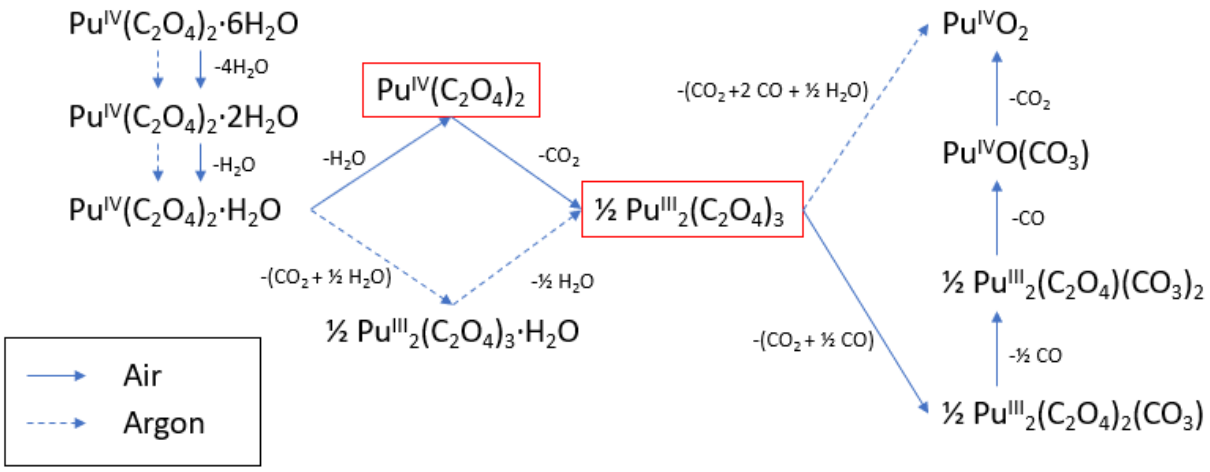

Scheme 1: Proposed reaction pathway for the calcination of Pu(IV) oxalate.[7-8] Species of interest noted in red.

Our interest in this topic centers on how dehydration and metal reduction influence the structure and ultimately the mechanistic pathway imposed during decomposition. The inability to directly interrogate the intermediate Pu(III) and Pu(IV) oxalate structures (highlighted in red in Scheme 1) presents an interesting challenge for theoretical methods to confirm their stability. While little is known about these anhydrous species, insights can be gleaned from their hydrated counterparts, shown in Figure 1. Pu(III) oxalate decahydrate is best characterized as forming a 2D honeycomb structure and crystallizes in the $P2_1/c$ space group.[9] On the other hand, the structure of Pu(IV) oxalate hexahydrate is not known but thought to be isostructural to the known U(IV) and Np(IV) analogs which crystallize in the *C2/m* space group with a 2D square lattice.[10] Other interesting structural changes are noted in the uranium and thorium analogs of the Pu(IV) oxalate hydrated species.[10] As seen in transition metal-organic frameworks, the angle of the oxalate molecules allow for geometric distortions during dehydration. In the case of the U(IV) and Th(IV) oxalate systems, a change from a nearly cubic AnO_8 geometry to a square antiprism geometry has been observed during dehydration. In the U(IV) oxalate dihydrate, the distance between the oxygen planes becomes shorter and the water molecules integrate into the coordination environment of the U, allowing for a bicapped square antiprism geometry.[11] The monohydrate U(IV) oxalate structure shows that the uranium atom is moved from the center of the AnO_2 framework towards the oxygen atom of the water to form a mono-capped square antiprism. Finally, in Th(IV) oxalate tetrahydrate, the bidentate oxalate units form two types of chains that interconnect to build a 3D framework.[12]

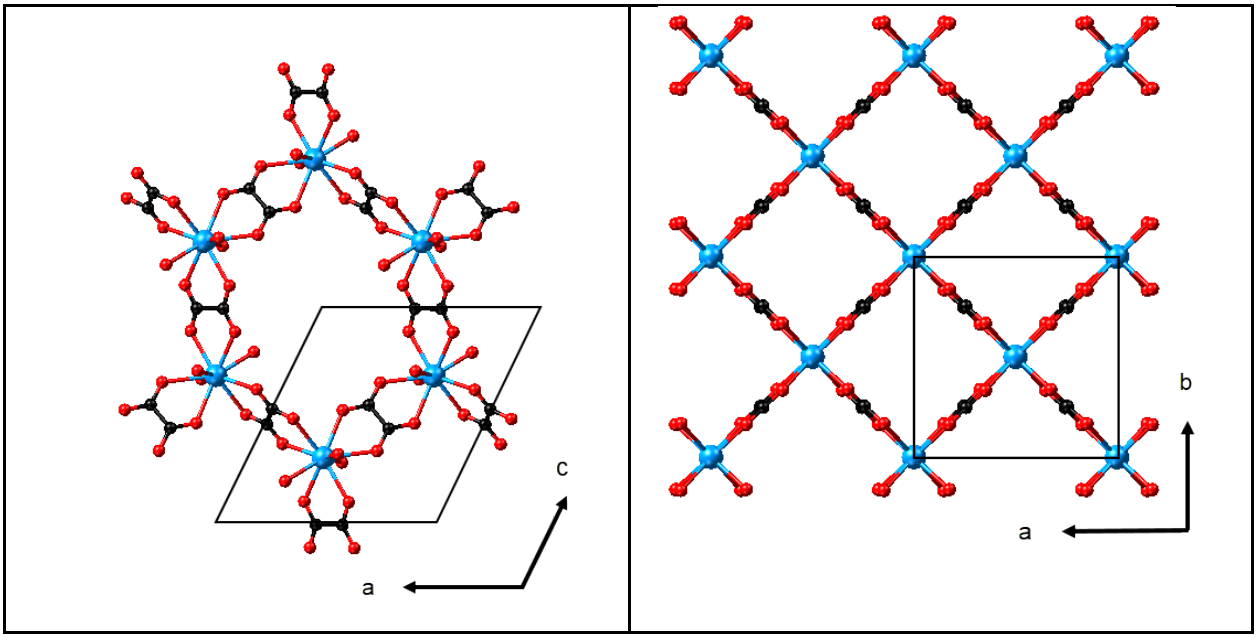

Figure 1: Two-dimensional networks of Pu(III) oxalate decahydrate (left) and U(IV) oxalate hexahydrate (right). Uncoordinated water molecules and hydrogen atoms are omitted for clarity. The color scheme for plutonium, carbon, and oxygen atoms as blue, black, and red, respectively, are carried throughout the paper.

Using the hydrate structures as a starting point, this paper will focus on the crystallographic and structural changes occurring for dehydrated Pu(IV) and Pu(III) oxalates. The resulting

energies will then outline the most likely reaction pathway based on thermodynamics. The structural parameters will also be analyzed and compared to identify trends in the bonding character of the ligands attached to the central plutonium atoms.

2: Computational Methodology

All calculations were performed using Kohn-Sham DFT calculations via the VASP 5.4 solid state chemistry program,[13] as integrated in the MedeA® computational environment. Exchange correlation potentials were described using the dispersion-corrected Perdew, Burke, Ernzerhof (PBE-D3) generalized gradient approximation (GGA) density functional.[14] The projector augmented wave (PAW) potentials described the valence electrons with the effective core, treating plutonium with 16 valence electrons ($6s^26p^67s^25f^56d^1$), carbon with 4 valence electrons ($2s^22p^2$) and oxygen with 6 valence electrons ($2s^22p^4$). The Pu potential included scalar relativistic effects for the core electrons. Electron correlation effects were accounted for through use of an effective Hubbard parameter U_{eff}[15] of 6 eV and J of 0 eV applied to the 5*f* orbitals on plutonium within the Dudarev formalism.[16] The integration in the reciprocal space over the Brillouin zone (BZ) was performed using a 2 × 2 × 2 Monkhorst-Pack mesh and a plane wave cutoff value of 400 eV was used for all calculations. Once the structure was fully relaxed, a denser Γ-point-centered 6 × 6 × 6 k-point grid was utilized to better describe the energies. The Pu ions were assumed to be antiferromagnetically coupled for all calculations based on the expected magnetic interaction of actinide ions coupling though an oxalate group. The magnetic moments were set to be antiparallel based on the 5*f* configuration of the Pu oxidation state for each structure.

3: Results and Discussion

3.1: Pu(IV) oxalate structural optimization

Although unknown, two possible structures are expected for dehydrated analogs of Pu(IV) oxalate, both exhibit a square lattice topology and are distinguished by the angle of the oxalate units linking the metal center.[10] The first structure is an analog of uranium(IV) and neptunium(IV) oxalate hexahydrate crystallizing in the *C2/m* space group wherein the metal center is surrounded by a nearly cubic coordination sphere of the oxygen atoms.[17] The second structure is an analog of the dihydrated oxalates possessing square antiprism geometry of the oxygens surrounding coordination center.[11, 18] These structures acted as the basis for optimization of the anhydrous forms labeled **Pu(IV)Ox-1** and **Pu(IV)Ox-2** in Figure 2. In addition, the oxalate ligand allows for κ denticity with the metal center, as illustrated in Scheme 2.

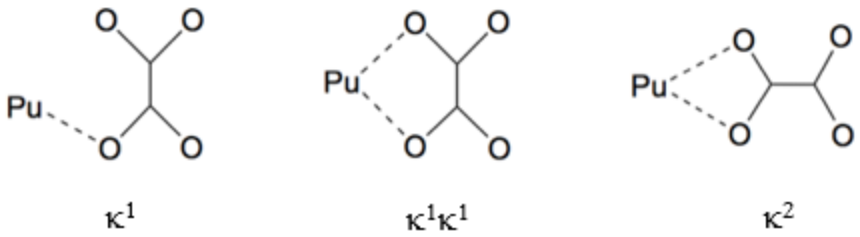

Scheme 2: Diagram of κ^1, κ^1,κ^1, and κ^2 denticity exhibited by the oxalate ligands in the optimized structures.

The first structure **Pu(IV)Ox-1** (Figure 2a) optimized to a monoclinic *C2/m* crystal structure with cell parameters *a*=8.51 Å, *b*=8.87 Å, *c*=5.19 Å, and β=107.10°. The structure was

further relaxed to *P1* and maintained the monoclinic parameters. Comparing to its hexahydrate analog, contraction along the (0 0 1) plane leads to a volume reduction of ~42% and interlayer distance of ~2.28 Å, suggesting no significant chemical interaction between the layers. The oxalate ions are nearly perpendicular to the (0 0 1) Miller plane and form a nearly cubic geometry around the Pu atom. Figure 3 shows the Pu-O bond distances of ~2.35 (±0.03) Å with κ^1,κ^1-binding mode of the oxalate ligands.

The second structure, **Pu(IV)Ox-2**, is 8.2 kJ·mol^{-1} higher in energy and retains a 2D topology. The structure first optimized in a monoclinic *P2/c* system and then relaxed to a triclinic system with lattice parameters of *a*=9.19 Å, *b*=7.07 Å, *c*=4.28 Å, α=90.04°, β=90.29°, and γ=85.51° (Figure 2b). Structurally, the metal center is located on the face of a distorted square antiprism formed by the oxygen atoms on the oxalate groups. The substantial tilt from the oxalate ions causes significant variation in the Pu-O bond distances. The charge bond oxygens all sit within 2.32-2.35 Å from their bonding plutonium atoms. The remaining Pu-O distances are within the ranges of 2.41-2.43 Å and 2.67-2.69 Å (Figure 3), more closely corresponding to a dative and/or nonbonding relationship of monodentate κ^1 binding versus the clear κ^1,κ^1 binding scheme in **Pu(IV)Ox-1**. The more compact structure leads to layers that are tightly stacked with a distance of ~1.57 Å. Comparison of the two suggests that the latter will have stronger chemical interaction between the layers based on the tighter crystal packing.

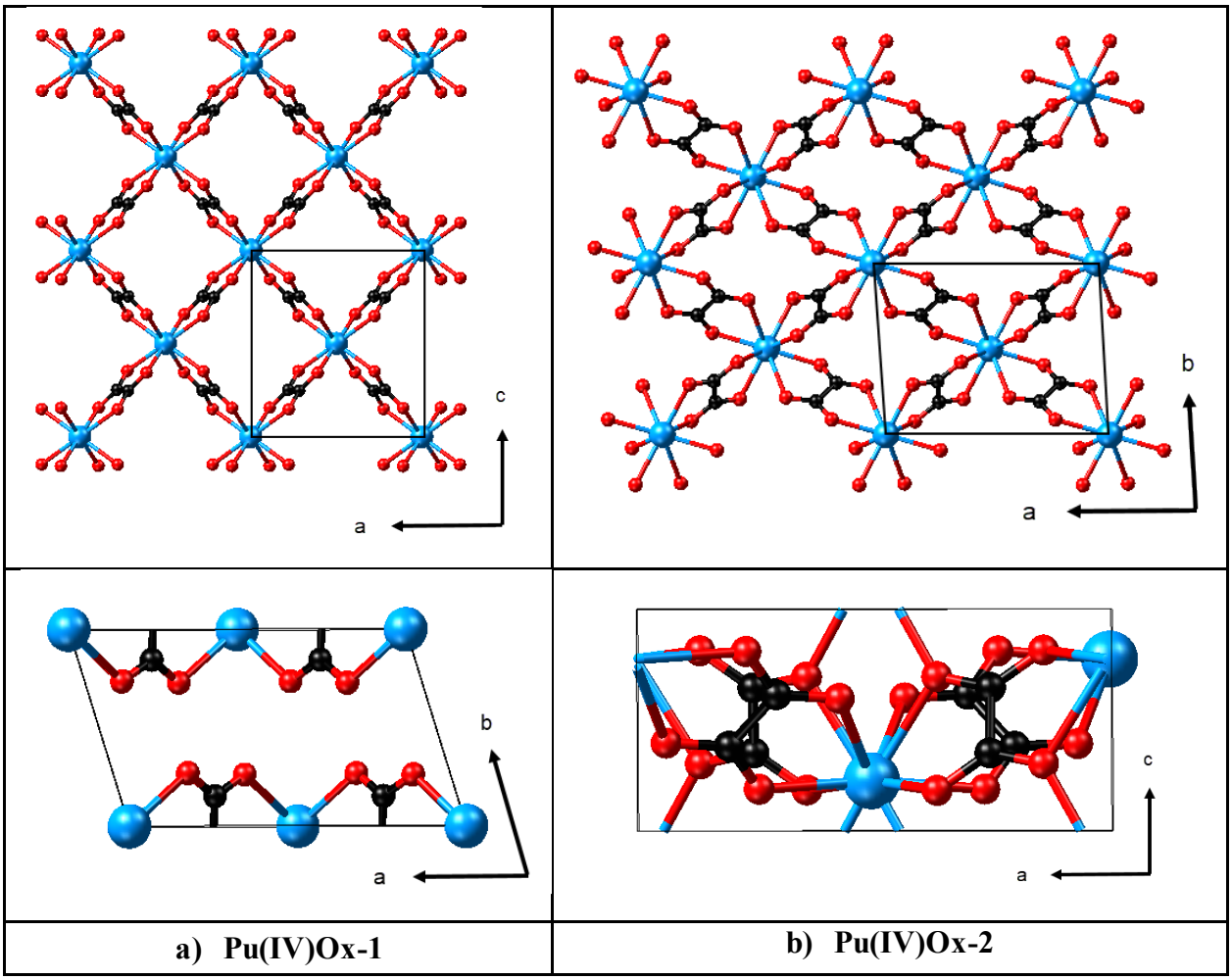

a) Pu(IV)Ox-1 **b) Pu(IV)Ox-2**

Figure 2: Comparison of optimized structures of a) **Pu(IV)Ox-1** and b) **Pu(IV)Ox-2** showing the 2D sheet topology and layer stacking (top and bottom, respectively).

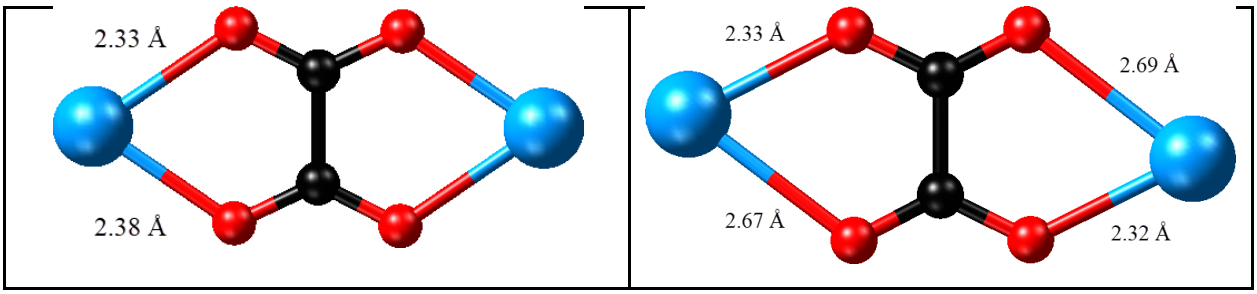

Figure 3: Representative Pu-O bond distances for **Pu(IV)Ox-1** (left) and **Pu(IV)Ox-2** (right).

3.2: Pu(III) oxalate structural optimization

During the first decarboxylation step under air (Scheme 1), an oxalate ligand decomposes to form CO_2 and a presumed Pu(III) structure. The aforementioned Pu(IV) structures were used to optimize two Pu(III) intermediates depending upon CO_2 release, labeled **Pu(III)Ox-1** and **Pu(III)Ox-2** in Figure 4. **Pu(III)Ox-1** optimized to a monoclinic $P2_1/c$ system with lattice parameters of a=11.14 Å, b=8.65 Å, c=9.67 Å, and β=118.08°; the structure remained monoclinic upon further relaxation of symmetry constraints (Figure 4a). It is structurally reminiscent of the plutonium(III) oxalate decahydrate crystal structure with a 19% volume reduction and shorter Pu-O bonds by ~0.1 Å. The 2D honeycomb topologies are shifted in the subsequent layers and there is an interlayer distance of 1.64 Å. The Pu-O bond distances range from 2.4-2.6 Å with the oxalate ligands exhibiting κ^1,κ^1 binding.

The second structure **Pu(III)Ox-2** (Figure 4b) is best described as 2D sheets conjoined via bridging oxalates to form a 3D network. It is 27.3 kJ·mol^{-1} higher in energy with monocyclic $P2_1/c$ lattice parameters of a=9.58 Å, b=7.92 Å, c=9.83 Å, and β=125.95°; it was further relaxed but retained the unit cell parameters. It still has void spaces but is more compact than **Pu(III)Ox-1** by ~200 Å^3. Further examination of the 2D sheet shows an unusually frustrated network of oxalate ligands binding to four Pu centers (Figure 5) ranging from ionic (~2.34 Å) to dative (~2.78 Å) bonds. The oxalate ligands exhibit both κ^1,κ^1 and κ^2 binding.

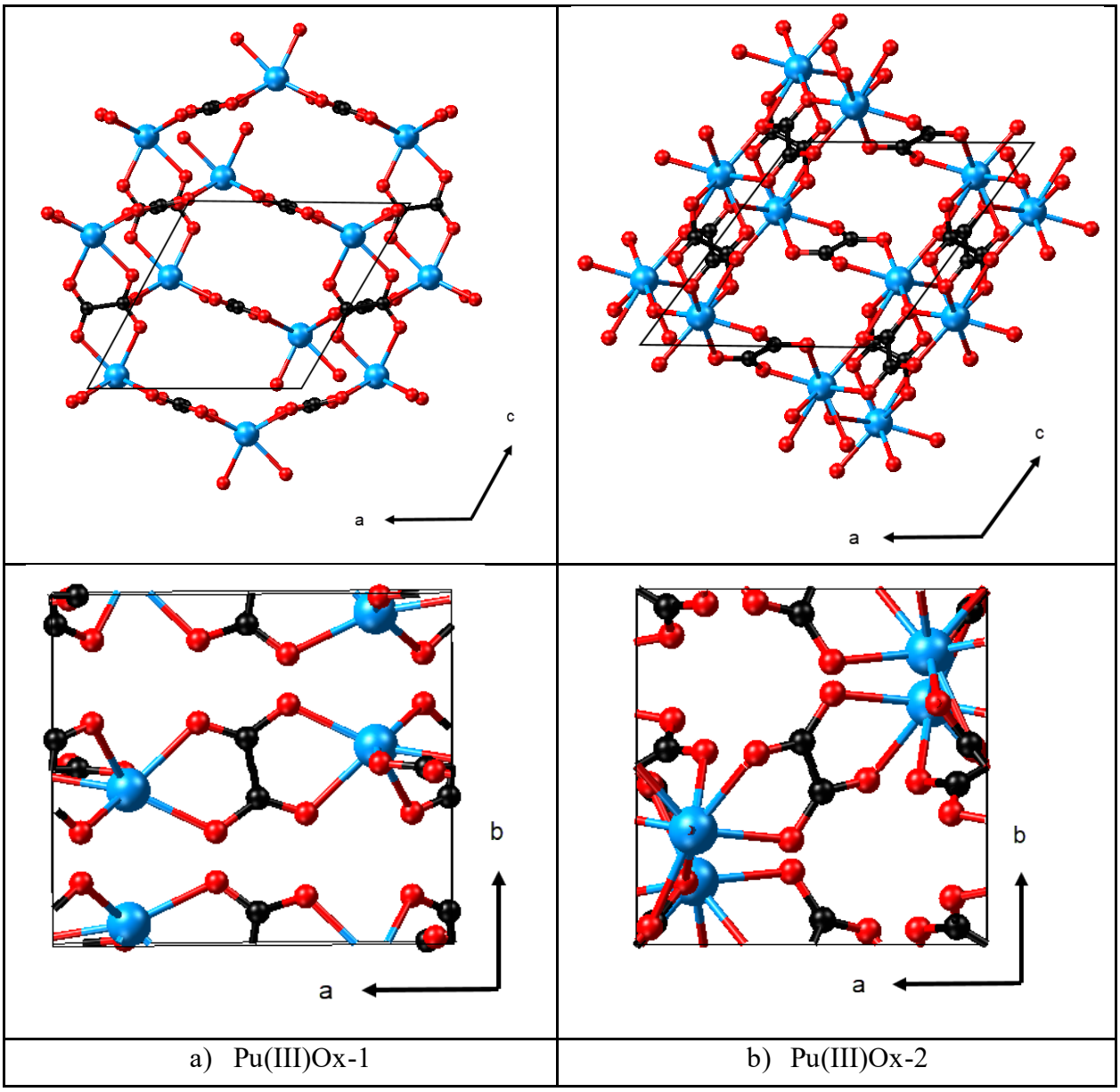

a) Pu(III)Ox-1 b) Pu(III)Ox-2

Figure 4: Comparison of optimized structures of a) **Pu(III)Ox-1** and b) **Pu(III)Ox-2** along the (0 1 0) and (0 0 1) Miller planes (top and bottom, respectively).

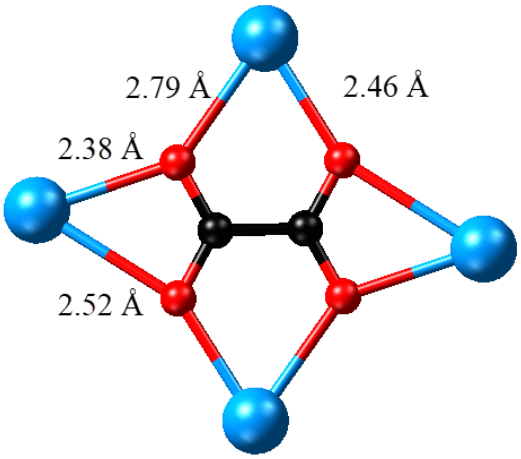

Figure 5: Pu-O distances of the frustrated oxalate binding to Pu in **Pu(III)Ox-2**.

When comparing the structures and calculating reaction energetics, differences among the sets are small with the lowest energy structures, **Pu(IV)Ox-1** and **Pu(III)Ox-1**, being the presumed local minima for the decomposition pathway. Table 1 shows the calculated reaction energies for each structure combination with the preferred reaction pathway being -133.8 kJ mol^{-1}. In all cases, the exothermicity of the reaction is consistent with experimental observations in the lack of a barrier toward the decomposition of the Pu(IV) oxalate to form the target intermediate Pu(III) oxalate.

Table 1: Calculated reaction energies for the reaction Pu(IV)Ox → Pu(III)Ox + CO_2 in kJ mol^{-1}.

	Pu(III)Ox-1	**Pu(III)Ox-2**
Pu(IV)Ox-1	-133.8	-106.5
Pu(IV)Ox-2	-142.0	-114.7

Interestingly, **Pu(IV)Ox-2** is only 8.2 kJ mol^{-1} higher in energy, leading to a total reaction energy of -142.0 kJ mol^{-1} for the conversion of **Pu(IV)Ox-2** to **Pu(III)Ox-1**. PBE-D3 has a mean absolute error on the order of kcals for atomization energies and is unfortunately not a rigorous enough computational method to be able to resolve these small energy difference.[19] Hence we expect a dehydrated Pu(IV) oxalate is dictated by the AnO_8 geometry and interlayer separation, and in the following reduction step to Pu(III) oxalate, there is a preference to lose CO_2 radical fragments within the 2D sheets rather than between crystal planes. This leads to an interesting consequence during the decomposition of Pu(IV) oxalate. As shown in Figure 2a, the 2D honeycomb lattice is shifted in the subsequent layers of **Pu(III)Ox-1**. Neither optimized Pu(IV) oxalate possesses this kind of repeat unit among the layers and as a result, would be expected to undergo a glide plane shift upon reduction to the **Pu(III)Ox-1** structure. Additionally, the Pu(IV)$(C_2O_4)_2$ formula units would have to break/recombine to form the honeycomb lattice found in **Pu(III)Ox-1**. Therefore, it is difficult to expect a significant geometric rearrangement within the plane or in the 2D lattice for either **Pu(IV)Ox-1** or **Pu(IV)Ox-2** structure in order to generate **Pu(III)Ox-1** even at temperature ranges of 200-250°C. However, if these same lattice arguments were applied to the higher energy structure **Pu(III)Ox-2**, no such rearrangements of the plutonium ions would be required save for small perturbations resulting from the new crystal field interactions surrounding

each plutonium ion. The difference would be arguments favoring the formation of a 3D structure with a frustrated oxalate binding to the Pu(III); a scenario entirely plausible during structure decomposition. Additional calculations are necessary to quantify either energy pathway and whether the path is thermodynamically or kinetically driven.

4: Conclusions

In summary, this work examined the dehydrated structures of plutonium oxalate to better understand the structural transition which could occur and highlighted important features which may outline the thermodynamic/kinetic pathways leading to decomposition to PuO_2. The dehydrated Pu(IV) oxalate results suggest the structure could be dictated by the AnO_8 geometry and interlayer separation. However, these structural differences are relatively small and reside on the same energy scale. On the other hand, the dehydrated Pu(III) oxalate structure could be akin to its decahydrate analog and exhibit a 2D honeycomb-like structure or lose CO_2 in the crystal plane to form a complicated 3D lattice structure with frustrated oxalate binding. These structural changes are key points in the decomposition. The energetics suggest the overall decomposition of Pu(IV) oxalate tentatively proceeds from **Pu(IV)Ox-1** to **Pu(III)Ox-1** based on thermodynamic arguments. However, one of the crystal planes of the former will need to undergo a shift and bond breaking/recombination in order to properly assume the crystal structure of the latter. More significantly, the reaction could proceed to form **Pu(III)Ox-2**, which is higher in energy but structurally very similar to the Pu(IV) oxalate identified in this study. Based on these results, continuing work will examine the structural pathway including entropic effects, transition state calculations, and kinetic studies to identify the intermediate species in plutonium oxalate decomposition.

5: Supplementary Information

Input files, structural information, XRD diffraction patterns, total energies

6: Acknowledgements

This work was funded by the U.S. Department of Homeland Security (DHS), Domestic Nuclear Detection Office (DNDO), under a competitively awarded Interagency Agreement No. HSHQDN-16-X-00054. Savannah River National Laboratory is operated by Savannah River Nuclear Solutions, LLC, for the U.S. Department of Energy under Contract No. DE-AC09-08SR22470. The United States Government retains and the publisher, by accepting this article for publication, acknowledges that the United States Government retains a non-exclusive, paid-up, irrevocable, worldwide license to publish or reproduce the published form of this work, or allow others to do so, for United States Government purposes.

7: References

1. Orr, R. M.; Sims, H. E.; Taylor, R. J., A review of plutonium oxalate decomposition reactions and effects of decomposition temperature on the surface area of the plutonium dioxide product. J. Nucl. Mater. **2015,** 465, 756-773.
2. Myers, M. N. Thermal Decomposition of Plutonium(IV) Oxalate and Hydrofluorination of Plutonium(IV) Oxalate and Oxide; HW-45128 United States 10.2172/4181389 NTIS HNF English; ; General Electric Co. Hanford Atomic Products Operation, Richland, Wash.: 1956; p Medium: ED; Size: Pages: 30.
3. Rao, G. S.; Subramanian, M. S.; Welch, G. A., Thermal decomposition of plutonium oxalates. Journal of Inorganic and Nuclear Chemistry **1963,** 25 (10), 1293-1295.

4. Jenkins, I. L.; Waterman, M. J., The thermal decomposition of hydrated plutonium(IV) oxalates. J. Inorg. Nucl. Chem. **1964,** 26 (1), 131-137.
5. Glasner, A., Remarks on the thermal decomposition of plutonium (IV) oxalates. J. Inorg. Nucl. Chem. **1964,** 26 (8), 1475-1476.
6. Nissen, D. A., The thermal decomposition of Plutonium (IV) oxalate hexahydrate. J. Therm. Anal. **1980,** 18 (1), 99-109.
7. Vigier, N.; Grandjean, S.; Arab-Chapelet, B.; Abraham, F., Reaction mechanisms of the thermal conversion of Pu(IV) oxalate into plutonium oxide. J. Alloys Compd. **2007,** 444-445, 594-597.
8. De Almeida, L.; Grandjean, S.; Vigier, N.; Patisson, F., Insights into the Thermal Decomposition of Lanthanide(III) and Actinide(III) Oxalates – from Neodymium and Cerium to Plutonium. Eur. J. Inorg. Chem. **2012,** 2012 (31), 4986-4999.
9. Runde, W.; Brodnax, L. F.; Goff, G.; Bean, A. C.; Scott, B. L., Directed Synthesis of Crystalline Plutonium(III) and (IV) Oxalates: Accessing Redox-Controlled Separations in Acidic Solutions. Inorg. Chem. **2009,** 48 (13), 5967-5972.
10. Abraham, F.; Arab-Chapelet, B.; Rivenet, M.; Tamain, C.; Grandjean, S., Actinide oxalates, solid state structures and applications. Coord. Chem. Rev. **2014,** 266-267, 28-68.
11. Clavier, N.; Hingant, N.; Rivenet, M.; Obbade, S.; Dacheux, N.; Barré, N.; Abraham, F., X-Ray Diffraction and μ-Raman Investigation of the Monoclinic-Orthorhombic Phase Transition in Th1−xUx(C2O4)2·2H2O Solid Solutions. Inorg. Chem. **2010,** 49 (4), 1921-1931.
12. Ziegelgruber, K. L.; Knope, K. E.; Frisch, M.; Cahill, C. L., Hydrothermal chemistry of Th(IV) with aromatic dicarboxylates: New framework compounds and in situ ligand syntheses. J. Solid State Chem. **2008,** 181 (2), 373-381.
13. (a) Kresse, G.; Furthmüller, J., Efficient iterative schemes for ab initio total-energy calculations using a plane-wave basis set. Physical Review B **1996,** 54 (16), 11169-11186; (b) Kresse, G.; Joubert, D., From ultrasoft pseudopotentials to the projector augmented-wave method. Phys. Rev. B **1999,** 59 (3), 1758-1775.
14. Perdew, J. P.; Burke, K.; Ernzerhof, M., Generalized Gradient Approximation Made Simple. Phys. Rev. Lett. **1996,** 77 (18), 3865-3868.
15. Anisimov, V. I.; Zaanen, J.; Andersen, O. K., Band theory and Mott insulators: Hubbard U instead of Stoner I. Phys. Rev. B **1991,** 44 (3), 943-954.
16. Dudarev, S. L.; Botton, G. A.; Savrasov, S. Y.; Humphreys, C. J.; Sutton, A. P., Electron-energy-loss spectra and the structural stability of nickel oxide: An LSDA+U study. Phys. Rev. B **1998,** 57 (3), 1505-1509.
17. Duvieubourg-Garela, L.; Vigier, N.; Abraham, F.; Grandjean, S., Adaptable coordination of U(IV) in the 2D-(4,4) uranium oxalate network: From 8 to 10 coordinations in the uranium (IV) oxalate hydrates. J. Solid State Chem. **2008,** 181 (8), 1899-1908.
18. Grigor'ev, M. S.; Charushnikova, I. A.; Krot, N. N.; Yanovskii, A. I.; Struchkov, Y. T., Crystal structure of neptunium(IV) oxalate hexahydrate Np(C2O4)2.6H2O. Radiochemistry (Moscow)(Transl. of Radiokhimiya) **1997,** 39 (5), 420-423.
19. Hermet, J.; Adamo, C.; Cortona, P., Towards a Greater Accuracy in DFT Calculations: From GGA to Hybrid Functionals. In Quantum Simulations of Materials and Biological Systems, Zeng, J.; Zhang, R.-Q.; Treutlein, H. R., Eds. Springer Netherlands: Dordrecht, 2012; pp 3-15.

Table of Contents

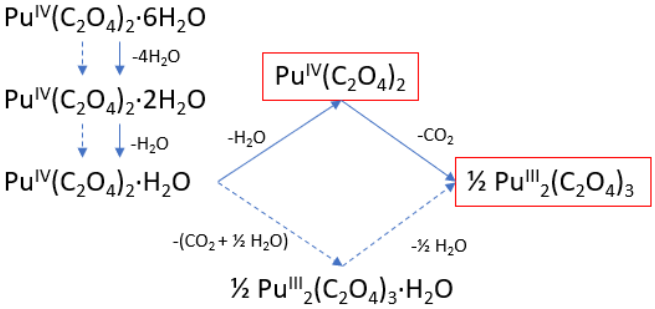

The intermediate structures $Pu^{IV}(C_2O_4)_2$ and $Pu^{III}_2(C_2O_4)_3$ during the thermal decomposition of Pu(IV) oxalate to PuO_2 was modeled in the solid state using DFT and an empirical correction for the band gap. The calculated energies for the target structures were then compared and used to identify the key crystal structures involved in the decomposition reaction.